J Mater Sci: Mater Electron (2017) 28:2290–2306
DOI 10.1007/s10854-016-5753-1

REVIEW

Kesterite-based next generation high performance thin film solar cell: current progress and future prospects

Zhengqi Shi[1] · Dinesh Attygalle[1] · Ahalapitiya H. Jayatissa[1]

Received: 25 February 2016 / Accepted: 27 September 2016 / Published online: 3 October 2016

Abstract Kesterites, $Cu_2ZnSn(S,Se)_4$ (CZTSSe) and Cu_2ZnSnS_4 (CZTS), have been considered as highly prospective candidates for solar cell applications. The non-toxic and earth-abundant elements along with tunable bandgap of CZTSSe indicate a high potential to replace the reported high efficient $Cu(In,Ga)(S,Se)_2$ and CIGS/CIGSSe devices in order to meet the increasing demand of solar cell market. In this review, the structural, optical and electrical properties of CZTS/CZTSSe were analyzed based on recent research in this field. Various vacuum/non-vacuum CZTS/CZTSSe synthesis and fabrication routines were also analyzed. The vacuum based deposition methods have yielded an efficiency of 11.6 % solar cells, while the non-vacuum paths, especially the ink-based approach offered a more convenient synthesis and fabrication choice with an advanced efficiency of 12.6 %. Analysis indicated that the barriers to application of this material system is still remained in both material synthesis and device fabrication. Further elucidation on possible mechanism of solution-based synthesis and some of the key barriers of improving the device efficiency are required to being pushed forward.

1 Introduction

Photovoltaic (PV) materials and devices have attracted great attention within past few decades due to the growing shortage of one-time fossil fuels and the corresponding global warming. Despite its clean and convenient nature, the price of solar power electricity is being more competitive with conventional powers than before. Until the third quarter of 2015, the price of photovoltaics has decreased from $76.67/Watt in 1977 to $0.67/Watt based on polysilicon PV cell [1]. Similar dropping of price was also reported in Europe: the photovoltaic system price had already dropped down of about 75 % in less than 10 years. In addition, a minimum of 40 GW annual PV installation and a worldwide 178 GW capacity at 2014 are reported [2]. These trends indicated the 'Swanson's law', which is a similar prediction as Moore's law in electronics field. The Swanson's law claims that the price of solar photovoltaic cells would fell 20 % for every doubling of industry capacity [3]. Currently, the mainstream of industrial PV technology is still based on Si-wafer, which occupied 92 % of the total 2014 annual PV production [4]. The corresponding mature technologies, similar to the integrated circuit industry, also contributed to the current occupation of this first generation PV materials. Even though the second and third generation PV materials and structures have already been developed, their efficiency and unit price cannot still challenge the dominate position of the single or poly-Si solar cells at present, especially after the overproduction of poly-Si and c-Si since 2009, which leaded to a market shakeout [5].

However, the disadvantages of c-Si are that it has an indirect bandgap. This requires a thick absorption layer at around 0.1 mm. Moreover, this thick layer enables more defects inside the layer: more grain boundaries, point defects and recombination centers. All of them could turn down the working efficiency of solar cells. On the contrary, other direct bandgap candidates with a higher absorption coefficient (10^4–10^5 cm^{-1}), such as CdTe and CIGS/Se, would need a much thinner absorber layer around several micrometers in the solar cell structure. This would largely prevents the negative effect

✉ Ahalapitiya H. Jayatissa
ajayati@utnet.utoledo.edu

[1] Nanotechnology and MEMS Laboratory, Department of Mechanical, Industrial, and Manufacturing Engineering, University of Toledo, Toledo, OH 43606, USA

from the defects. In fact, lab-scale solar cell s fabricated from those materials have been comparable with the Si-based cells, which reached an efficiency of 24.7 % on a size of 101.8 cm^2 [6]. For example, the current world record efficiency of CIGSe solar cell had reached to 21.7 % through co-evaporation at Stuttgart's Centre for Solar Energy and Hydrogen Research [7], First Solar, Inc. also successfully achieved an efficiency of 21.5 % on CdTe-based solar cells [8]. Moreover, trials on fabrication of those materials on flexible and non-glass substrates has also been developed [9].

The above progress indicates the conversion efficiency of thin film based the second generation PV has become comparable with c-Si. But another factor limiting the reduction of price is the toxicity of CdTe and the availability of indium and gallium. The amount of indium in the upper continental crust of earth is estimated to be 0.05 ppm (compared with an abundance of 25, 71 and 5.5 ppm for copper, zinc and tin, respectively) [10]. Current world-wide production capacity for indium is approximately 600 metric tons per year [11]. As a consequence, non-toxic PV materials with earth abundant elements need to be developed. A possible candidate is CZTS or CZTSSe where group III elements (In, Ga) of CIGS system were replaced by zinc and tin. Further research proves that CZTS shares similar optical and electrical properties with a suitable and tunable direct bandgap around 1.0–1.5 eV. Thus, the thin-film technologies developed for CIGS can readily be applied on fabrication of CZTS or CZTSSe solar cells.

Currently, chalcopyrite CZTSSe absorption layer have extensively been studied for solar cells. Those studies, together with progress in CZTS/CZTSe, would appear in this review. As a technology derived from CIGS technology, the CZTSSe solar cell structure uses the same structure of glass/Mo/CZTSSe/CdS/AZO from CIGS. The photovoltaic effect of CZTS was first demonstrated in 1988 [12]. Until 1997, the CZTS and CZTSe devices had already reached an efficiency of 2.3 % [13]. Katagiri et al. [14] improved the efficiency up to 5.7 % by optimizing the deposition method. For CZTSSe, a 7.2 % efficiency has been reported from Purdue University [15] and the current efficiency records are 9.15 % based on co-evaporation process [16] and 10.1 % based on a hydrazine-based solution method [17]. The latest record of CZTSSe solar cell had already jumped to an efficiency of 12.6 % demonstrated by IBM and Solar Frontier [18]. More details would be discussed in the device fabrication section.

2 Crystal structure and composition

It is accepted that CIGS/CIGSSe has a chalcopyrite structure. Thus, due to the similarity of CZTS and CIGS, it is also predicted that CZTS has a same structure as CIGS. However, further research shows two kinds of stable structures and both are possible for CZTS: chalcopyrite and CuAu-like structure. Moreover, there are also two CuAu-like structures: stannite (KS) and primitive mixed CuAu-like structure (PMCA) [19]. The major difference of those two stable structures are the locations of Cu and Zn. Moreover, PMCA structure shows a further partially disorder with Zn–Sn. Figure 1 shows more details about those three structures.

A detail calculation indicated that the KS structure is the ground state for CZTS/CZTSe while ST and PMCA structures have higher total energy. The results are shown in Table 1 [19]. Moreover, the KS structure has a lower strain energy [20] and a lower Madelung energy [21]. Thus, the actual CZTS/CZTSe structure is considered as a mixture of KS and ST structures due to the relatively smaller energy difference together with relevant experimental results. Even though the theoretical calculation based on the relativistic FPLAPW method indicated that the KS structure might be the right ground state for both CZTS and CZTSe [22], this effect increases the difficulty to identify the actual structure via traditional methods such as X-ray diffraction. In addition, the isoelectronic Cu^+ and Zn^{2+} could affect the X-rays and increase the hardness for XRD to distinguish those two structures [23]. Moreover, since the stannite structure is predicted with a smaller bandgap than kesterite structure, this mixed structure may lead to a lower open-circuit voltage in the solar cell [24]. However, there is still no agreement about the actual structure of CZTS and CZTSSe due to the nearly random location of Cu and Zn (Fig. 2).

Due to the complex composition of CZTS/CZTSe, different secondary phases would exist. According to the published phase diagrams for CZTS at 673 K [5], only a narrow region is allowable for pure CZTS. As summarized from Delbos [25], those record CZTS/CZTSe cells are all fabricated from a Zn-rich and Cu-poor composition. A common secondary phase in CZTS is ZnS according to the observation from Wibowo et al. [26]. Also, due to its wide

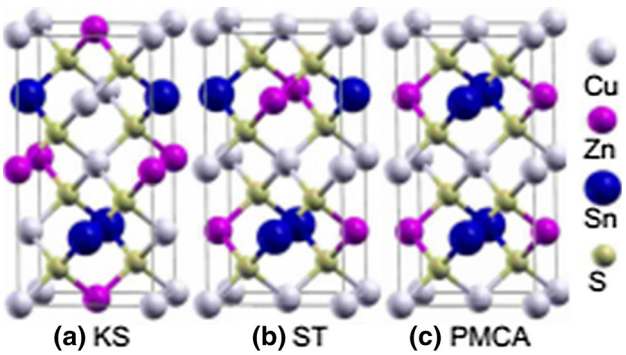

Fig. 1 The crystal structure of Cu_2ZnSnS_4 in **a** KS, **b** ST, and **c** PMCA structure [19]

Table 1 Calculated lattice constant α, tetragonal distortion parameter η, crystal field splitting Δ_{CF}, energy difference per atom ΔE, and direct bandgap (E_g) labeled in brackets after an HSE06 calculation correction on the original GGA calculation [19]

Structure	a (Å)	η	Δ_{CF} (eV)	ΔE (meV)	E_g (eV)
CZTS					
KS	5.467	0.999	−0.065	0	0.09 (1.50)
ST	5.458	1.004	0.138	2.86	−0.3 (1.38)
PMCA	5.459	1.005	0.128	3.15	−0.06 (1.35)
CZTSe					
KS	5.763	0.998	−0.031	0	−0.30 (0.96)
ST	5.762	1.000	0.066	3.79	−0.44 (0.82)
PMCA	5.753	1.004	0.065	5.53	−0.47 (0.79)

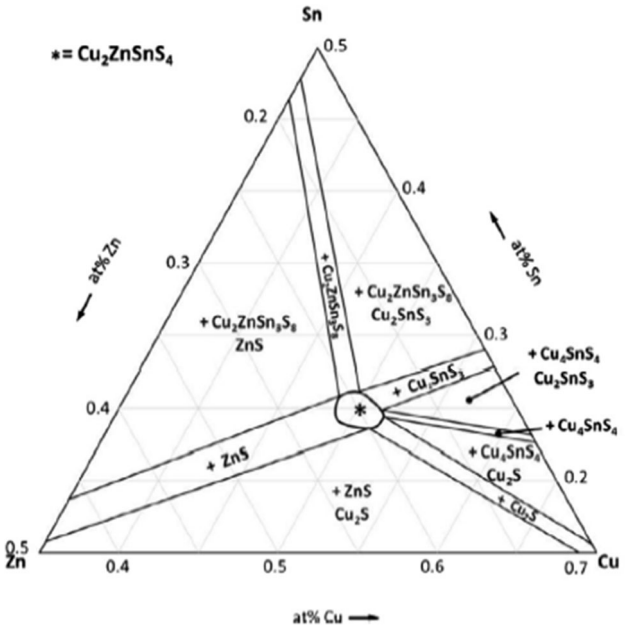

Fig. 2 CZTS ternary phase diagram with corresponding secondary phases at 673 K [5]

bandgap and relatively low conductivity, it would lead a higher cell resistivity to reduce voltage output [24].

3 Optical properties

A direct bandgap of kesterite CZTS and CZTSe was theoretically demonstrated as 1.5 eV and about 1.0 eV for perfect stoichiometric samples [19]. Thus, for CZTSSe, a tunable bandgap between 1.0 and 1.5 eV is expected. Figure 3 shows the calculated result by Fan et al. [27]. This result indicated a nearly linear relationship between the bandgap and the S/Se ratio in CZTSSe and the little impact from different crystal structures (less than 0.1 eV) on the bandgap. A further mathematical formula described the change of CZTSSe bandgap [28]:

$$Eg(X) = (1-x)E_g(\mathrm{CZTS}) + xE_g(\mathrm{CZTSe}) - bx(1-x)$$

where x is the ratio of Se/(Se + S) and b is a constant of 0.07. This effect may be due to the low energy cost to randomly replaced Cu and Zn cations in CZTSSe system, which is the only difference between those two crystal structures [29].

The coefficient has been estimated from the absorption spectra of CZTSSe powders. He et al. [30] measured the absorption spectra via UV–vis-NIR spectrophotometer and observed a blue shift at the band-edge absorptions when increasing sulfur amount. This result shown in Fig. 4 is due to the bandgap difference.

Another important parameter is the transmission which also has a strong relationship with bandgap. Figure 5 shows an experimental result of transmission spectra and the corresponding bandgap value is determined by extending the straight line of $(\alpha h\upsilon)^2$ versus photon energy curve to the horizontal axis [31]. From Fig. 5, it is shown that the optical bandgap values of thin films are slightly larger than the bulk samples with same composition. Moreover, this difference would be enlarged as the content of sulfur increases. Further XRD and Raman spectra demonstrated that the internal compressive stress is the reason [32] since this internal compressive stress would cause lattice shrink that affects the bandgap [33, 34].

4 Electrical properties

Unlike other conventional intrinsic semiconductor materials, CZTS/CZTSSe could achieve self-doping since the various defects formed during the synthesis and growth of CZTS or CZTSSe thin films. Chen et al. [35] studied the doping effect of defects in CZTS by first-principle

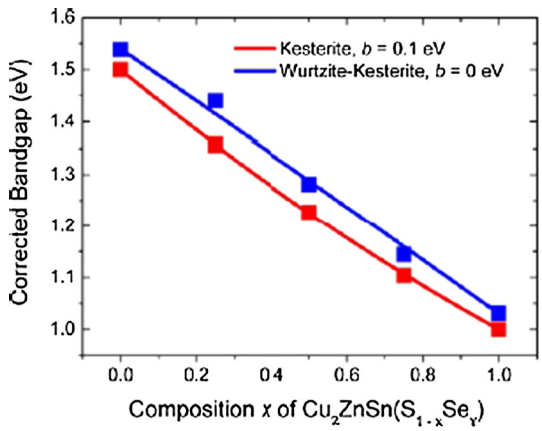

Fig. 3 Band-gap dependence of the wurtzite-derived (*blue*) and zincblende-derived (*red*) CZTSSe alloy on the composition x [27] (Color figure online)

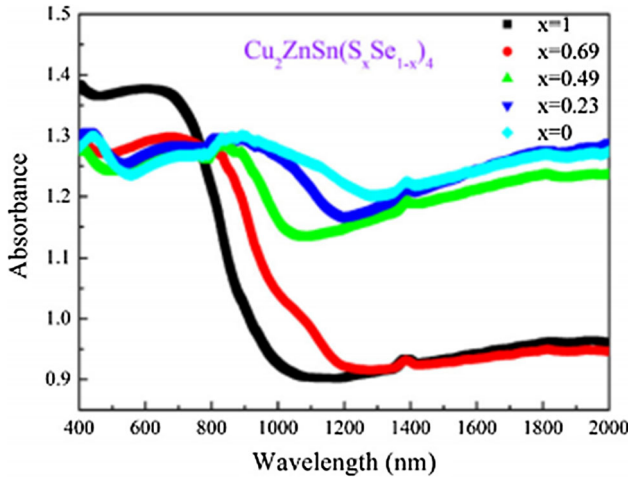

Fig. 4 Absorption spectra of $Cu_2ZnSn(S_xSe_{1-x})_4$ powders [30]

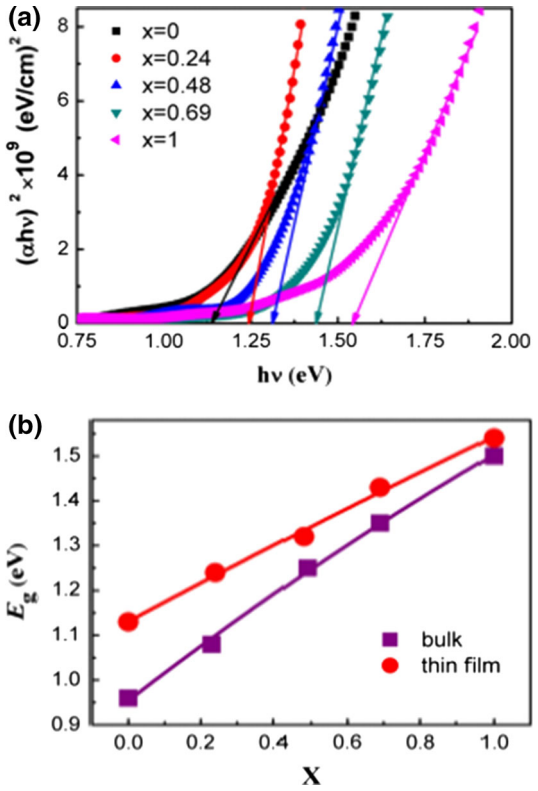

Fig. 5 **a** Optical bandgap determination from transmission spectra of $Cu_2ZnSn(S_xSe_{1-x})_4$ thin films with varying x values, **b** the optical bandgaps of CZTSSe thin films and CZTSSe bulks [32]

calculations based on a 64-atom supercell approach. They found that it was easier for CZTS to form acceptor defects than the donor defects. This indicated the CZTS would be naturally p-type. Other observation demonstrated the main source of doping was from the Cu_{zn} anti-site defect. This maybe explained the reason of applying copper-poor and zinc-rich relationship in initial synthesis for high-efficiency device fabrication process [15, 25].

Some groups also reported the carrier density, mobility and resistivity of as-synthesized CZTS/CZTSSe thin films. Some of the mobilities in Table 2 [24] were compatible with reported CIGSSe results [36]. However, the results were slightly different from group to group. The mobility, hole concentration (varies from 10^{16} to 10^{18} cm^{-3}) [37, 38], resistivity (from 10^{-3} to 10^{-1} Ω*cm) [50] of CZTS are lower than CIGS thin films, which indicates a thinner absorption layer should be considered when optimizing CZTS/CZTSSe solar cell structure. Since some results (especially those in Table 2) were from samples deposited on intrinsic substrate, those measurements did not fit the exact performance in the actual device. But it is still long way for CZTS/CZTSSe to meet the current record of CIGS/CIGSSe.

Most of the CZTS thin film solar cells were fabricated with a chemical-bath-deposited (CBD) CdS layer to form a hetero-junction. The conduction band offset between CZTS and CdS is 0.4–0.5 eV, which may exceed the optimal limitation of 0.4 eV and lead to a lower efficiency [39]. Moreover, it is better to avoid cadmium application due to the toxicity. Thus, some alternative buffer layer was applied such as In_2S_3, ZnS(O/OH) [40, 41]. However, the performance of corresponding devices was still lower than devices with CdS buffer layer.

5 Synthesis and fabrication of CZTS/CZTSSe: research highlights

Many synthesis and fabrication routines have been tried for CZTS/CZTSSe thin film deposition. These processes could be roughly divided into two groups: vacuum-based and non-vacuum-based. For both approaches, the major challenges are the synthesis of single CZTS/CZTSSe phase and precise control of Sn and Zn during the deposition process due to the volatility [42], which worsens the difficulty of composition control in the CZTSSe system.

5.1 Vacuum-based routine

Vacuum environment enables high potential of uniform deposition and generate reactions that cannot be accomplished under normal atmospheric condition. Therefore, high-quality thin film device is possible to be fabricated. However, those processes are relatively costly. The most commonly used are sputtering and co-evaporation, or a combination of these two technologies.

5.1.1 Sputtering

In 1988, Ito et al. [12] first used atom beam sputtering to synthesize CZTS thin films. This process required no

Table 2 Reported electrical properties of selected as-synthesized CZTS/CZTSSe thin film determined by Hall measurement

Compound	Carrier density (cm^3)	Mobility cm^2/Vs	Resistivity Ω cm
Cu_2ZnSnS_4	8.2×10^{18}	6.3	0.16
Cu_2ZnSnS_4	8.0×10^{18}	6.0	0.13
Cu_2ZnSnS_4	$>5 \times 10^{19}$	<0.1	>1.3
Cu_2ZnSnS_4	3.8×10^{18}	12.6	–
$Cu_2ZnSnSe_4$			0.1–0.8
$Cu_2ZnSnSe_4$	2.1×10^{17}	39.7	0.74

The 3rd row of CZTS was identified with a stannite structure while all other CZTS revealed a kesterite structure [24]

further treatment but the efficiency was not provided. Since then, more works focused on RF or DC sputtering of multi-layer metal or compound deposition. Lechner et al. [43] sputtered a uniform Cu/Zn/Sn stack with a total thickness of 600–800 nm onto rotated Mo-coated glass substrate. In addition, a thermal evaporation of Se and annealing under sulfur atmosphere helped forming final CZTSSe thin film. The final thin film has a Cu/(Zn + Sn) = 0.73 and Zn/Sn = 1.1 with a highest efficiency of 6.6 % [43]. Also, another opposite Sn/Cu/Zn stack was applied by DC sputtering on Mo-coated soda-lime-glass substrates without heating. After further annealing with S and Se powders under 200–550 °C followed by air cooling, the reported efficiency was 5.5 % [44], proving the metal precursor sequence won't largely affect the final CZTSSe formation. Moreover, a recent report pushed the efficiency to 8.1 % by further decreasing the ratio of Cu/(Zn + Sn) and increasing Zn/Sn. The CZT stacks were separately sputtered, rapid annealed only with Se and etched in 10 % KCN solution. Such etching helped to remove the ZnS secondary phase. The final device structure was SLG/Mo/CZTSe/CdS/i–ZnO/ZnO:Al [45]. Their work, as shown in Fig. 6 [45], also emphasized that Cu-poor and Zn-rich composition was the key to achieving higher efficiency CZTSSe solar cell (Table 3).

An alternative choice was replacing the elemental source into compounds appeared as the secondary phase in CZTS/CZTSSe system. Some improvements had been approached by far. Katagiri's group achieved an efficiency of 5.74 % [46] used RF-sputtering with Cu, ZnS and SnS precursors and after rotating deposition, the samples were annealed for 3 h under $H_2S + N_2$ atmosphere to finish sulfurization. Further work suggested a lower H_2S concentration since it is highly corrosive to the reaction chamber and meanwhile, different H_2S percentage affected very little on final device characterizations. Moreover, a best element composition of achieving high device efficiency was also demonstrated according to their further work: Cu/(Zn + Sn) ≈ 0.9, Zn/Sn ≈ 1.25 [47]. In a later research, a ZnS/Cu/Sn stack was applied but only ZnS was deposited by RF sputtering while other two precursors were

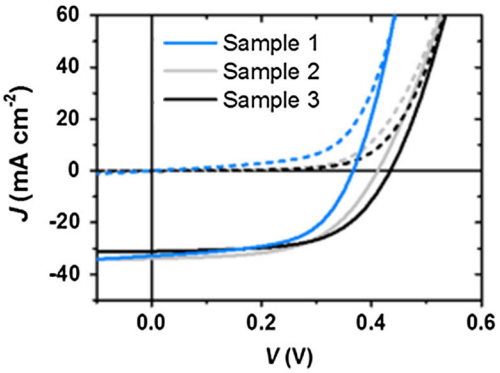

Sample	V_{oc} (mV)	J_{sc} (mA/cm²)	FF (%)	Eff (%)	E_g (eV)
Sample 1	367	33.0 (33.3)	56.8	6.9	1.00
Sample 2	411	34.0 (34.1)	56.2	7.9	1.04
Sample 3	434	31.2 (32.8)	59.6	8.1	1.07

Fig. 6 Current–voltage characteristics of the best solar cells with three different stoichiometric ratio under AM1.5 illumination and the corresponding solar cell parameters. From sample 1 to 3, the Cu/(Zn + Sn) ratio kept decreasing while Zn/Sn ratio kept ascending in the absorption layer [45]

deposited via electron-beam evaporation. By varying the thicknesses of different precursors, the element ratio and final CZTSSe thickness were changed. The thinner sample had no problem in light absorption loss but showed a significantly lower shunt resistance and a lower efficiency of 4.1 % compared with 6.0 % efficiency of thicker samples [48].

Direct sputtering through quaternary targets was also considered in order to replace the multi-layer stack. He et al. [49] reported sputtering of a quaternary target with Cu_2S, ZnS, SnS_2 and S powder as the starting precursors. The molar ratio of Cu_2S:ZnS:SnS_2: S was 2:1.5:1:1. An additional post-annealing in Ar + H_2S (5 %) atmosphere at 520 °C was applied, which was demonstrated to offer a small increase of Cu and S component and decreased the bandgap. An important parameter was the substrate temperature that would affect both the chemical component and the crystal structure. By discarding the sulfur powder, Lin et al. [50] also prepared the single-phase CZTS target

Table 3 Interplanar spacing of (112) and crystallite size of as-deposited (above) and post-annealed (below) thin films with various substrate temperatures [49]

Sample ID	As-deposit temperature (°C)	Interplanar spacing of (112) (Å)	FWHM of (112) peak (deg)	Crystallite size (d) (nm)
As-deposited				
S-350	350	3.100	1.00	8
S-400	400	3.104	1.04	8
S-450	450	3.106	1.10	7
S-500	500	3.106	1.10	7
Post-annealed				
S-350	520	3.120	0.36	23
S-400	520	3.128	0.41	20
S-450	520	3.126	0.41	20
S-500	520	3.120	0.41	20

through CuS, ZnS and SnS_2 with a ratio: 1.6:1:1:4. The CZTS film was fabricated by sputtering and high-temperature post-sulfurizing. After KCN etching, the device was assembled with a structure of SLG/Mo/CZTS/CdS/i–ZnO/IZO/Al grid, where IZO was indium-doped ZnO. Although a stoichiometric ratio close to the ideal CZTS was examined rather than significant Cu-poor and Zn-rich, the best device fabricated under the highest vacuum showed an efficiency of 5.2 % with $Voc = 0.52$ V, $Jsc = 19.17$ mA/cm^2 and $FF = 52.7$ % (Figs. 7, 8).

Sputtering was among the earliest technique applied on CZTS/Se synthesis. By sputtering, the elemental ratio could be controlled in a straight forward way by varying each thickness in the stacks. However, unless a high-quality CZTS/Se could be sputtered from the direct target, sulfurization/selenization could never be skipped and binary/ternary phase formation can hardly be avoided. This created extra toxic etching steps (e.g. 10 % KCN solution, shown in Table 4) before the next step. Also, when it comes to an industrial manufacturing, the production period might become another negative factor (Fig. 9).

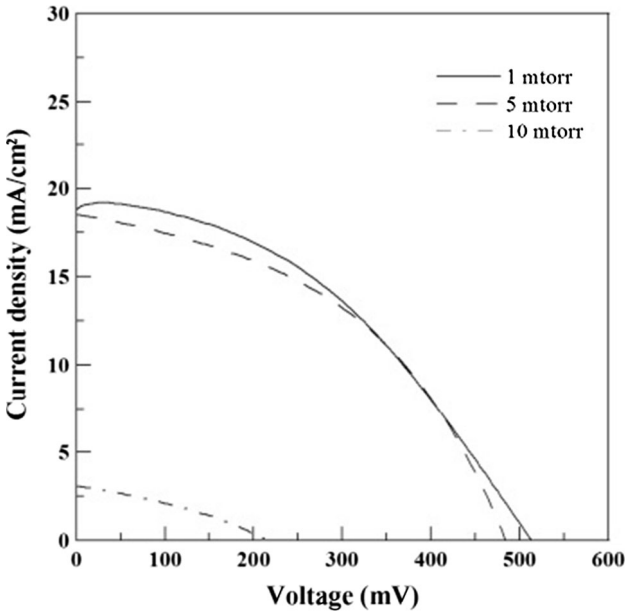

Fig. 7 J–V curve of CZTS solar cell fabricated under different pressure [50]

5.1.2 Evaporation

Another typical synthesis approach of the metal stack is evaporation. In 1997, Katagiri's group first fabricated an elemental stack on Mo-coated soda lime glass with a structure of Cu(180 nm)/Sn(230 nm)/Zn(160 nm) by sequentially evaporation [14]. The later sulfurization was held with $N_2 + H_2S$ (5 %) atmosphere. An open circuit voltage up to 400 mV and a device efficiency of 0.66 % were then reported [51]. They later replaced Zn with ZnS, a common secondary phase of CZTS system. Also various film thicknesses were deposited and the annealing temperature was increased from 500 to 550 °C [52]. The solar cell parameters in Table 5 indicated the negative effect of growing film thickness on short-circuit current density and the fill factor of the solar cell. A similar effect of film thickness was demonstrated: A series of elemental sources of Cu, Zn, Sn and S were applied for co-evaporation onto SLG/Mo substrate at about 110 °C. Moreover, the following 5 min sulfurization instead of previous hourly annealing with S was another highlight advantage of this report. Later analysis indicated that a high series resistance from the blocking back contact may be responsible for the efficiency limitation [53]. This co-evaporation path was also applied on the synthesis of CZTSe films by replacing Se with S. An additional 5 min Zn flux was applied by the end of co-evaporation to maintain a Zn-rich CZTS thin film. However, it is

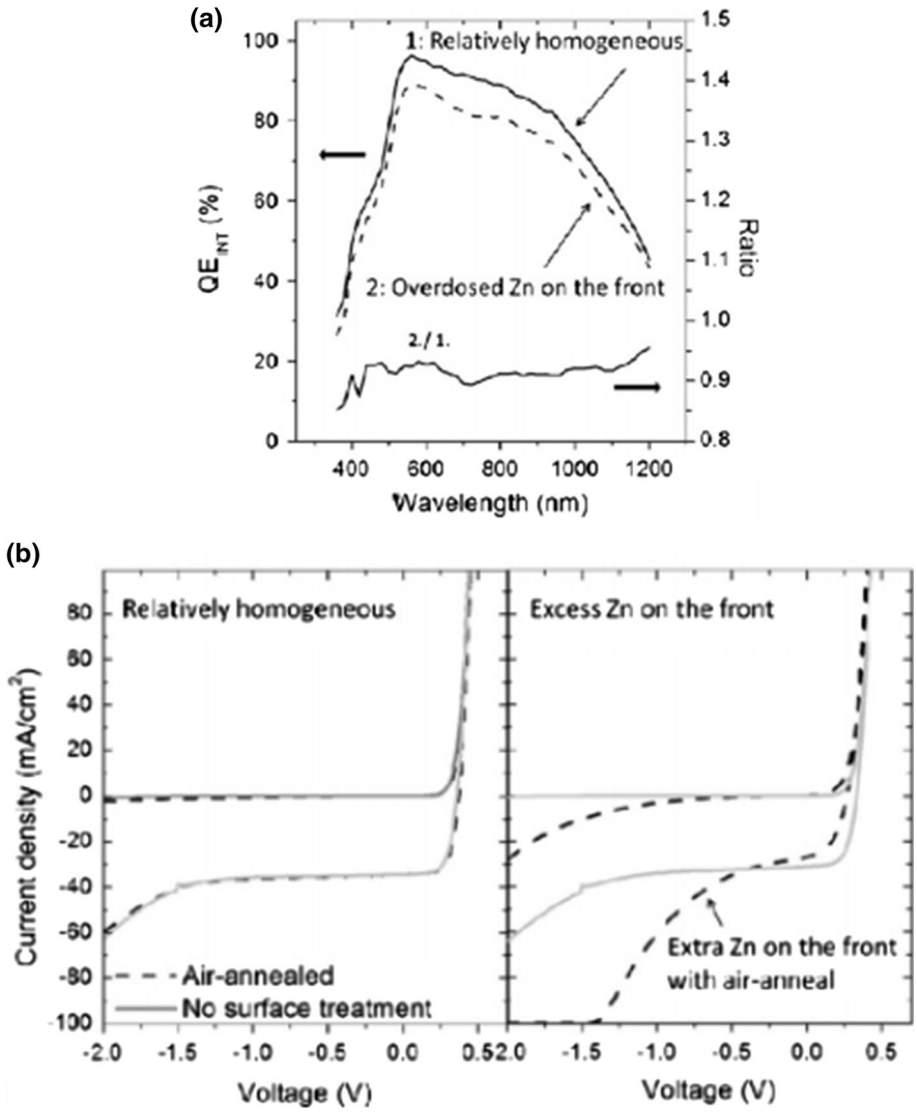

Fig. 8 **a** Quantum efficiency of stoichiometric devices and devices with ZnSe grains on the front of absorber and the ratio between them. **b** J–V curves of the same two devices and their air-annealed counterparts [54]

Table 4 Information about sputtering deposition method

Sputtering approaches	Precursor details	Post treatment	Efficiency	Ref.
DC-sputtered metal stack	Cu/Zn/Sn Stack on Mo/SLG	Se layer is thermal evaporated + Annealing with S	6.6 %	[43]
DC-sputtered metal stack	Sn/Cu/Zn stack on Mo/SLG	Annealing with S and Se powder	5.5 %	[44]
DC-sputtered metal stack	**Cu/Zn/Sn stack on Mo/SLG**	**Annealing with Se + KCN (10 %) Etching**	**8.1 % (record cell)**	[45]
RF co-sputtering	Cu + ZnS + SnS or Sn on Mo/SLG	Annealing in N_2 + H_2S(5 %)	5.74 %	[47]
RF-sputtering	ZnS/Cu/Sn with diff. thickness on Mo/SLG	Annealing with Se at 570 °C for 30 min	4.1−6.0 %	[48]
DC-sputtered quaternary target	Cu_2S + ZnS + SnS_2 powder	Annealing with Sulfur + KCN (10 %) Etching	5.2 %	[50]

The row in bold stands for the champion cell among all those reported results

referred that the Zn-rich phase (ZnSe) is only helpful useful for the back of the absorber layer. Otherwise the ZnSe would result in photo-current reduction and diode breakdown in lower reverse bias [54].

Another possible factor improves the device efficiency would be the role of sodium in the CZTS absorption layer. For example, Wang et al. [53] increased Na level by NaCS etching before depositing CdS layer. The detail

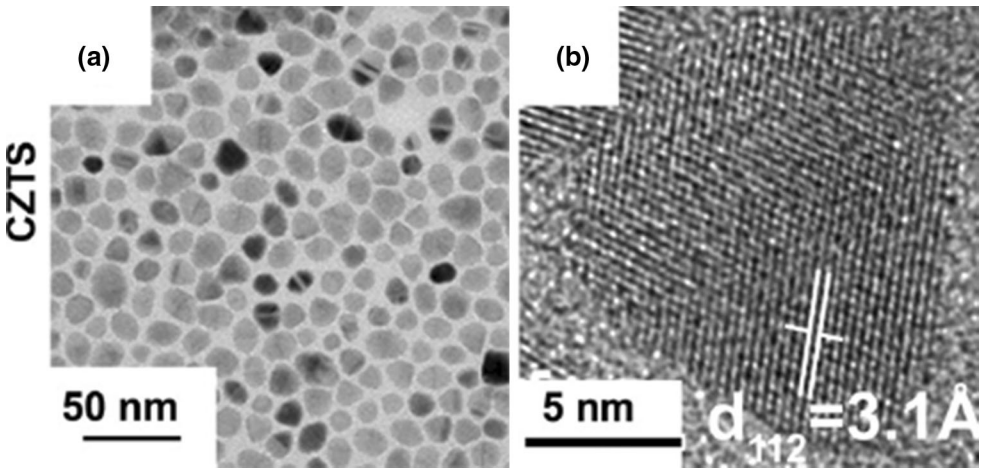

Fig. 9 TEM images of CZTS nano-crystals under different scales [58]

enhancement mechanism is still not clear. One assumption was that the Na could improve the CZTS surface and this enhancement was observed in another work: Jampana et al. deposited the films on SLG and borosilicate glass, which resist Na existence. The results showed the grain size and hole concentration of SLG sample was larger than the sample deposited on borosilicate glass due to Na diffusion. This diffusion also affected the electrical characteristics of device [55].

A novel sodium doping approach was accomplished by Mise et al. [56]. By applying a NaF layer before the elemental co-evaporation, their cell performance reached 5.23 %. Moreover, the current efficiency record of 11.6 %, reported by IBM at Dec. 2015 shown in Table 6 [57], was achieved by similar approach. These results made co-evaporation comparable to the current best CZTSSe solar cell with 12.6 % efficiency. This co-evaporation work went back to elemental starting sources on a 30 nm pre-deposited NaF layer. A pure selenite phase achieved by post-selenization. With observed increasing of minority carrier diffusion length, the carrier collection was enhanced and the J_{sc} was therefore, boosted to 40.6 mA/cm^2. This breakthrough indicated that the future focus should be better on pure CZTSe phase instead of the mixed CZTSSe for co-evaporation. However, the mechanism of sodium ion diffusion and its effect on solar cell performance need more in-depth discussion.

5.2 Non-vacuum routines

As discussed above, those vacuum based routines could synthesize CZTS/CZTSSe thin film by using straightforward precursors due to high energy and vacuum conditions. However, these requirements are also the barriers when applying to real industry. Thus, various non-vacuum approaches are being established and demonstrated a similar result as those vacuum-based methods.

5.3 Nano-particle ('ink') based approach

Nano-particle methods (also named 'colloidal techniques' or 'ink methods') have been demonstrated as an effective way to synthesize CIGS and CZTS. Generally speaking, the 'ink' contains nano-particles dispersed in particular solvent. In order to form the thin film, this suspension was coated on a substrate first. Then by heating or other paths, the solvents are evaporated. An example of synthesizing CIGS nano-crystals is shown below [58]:

$$\mathrm{CUCl} + (1-x)\mathrm{InCl_3} + x\mathrm{GaCl_3} + 2\mathrm{Se} \xrightarrow[[240\,^{\circ}\mathrm{C}]]{\text{oleylamine}} \mathrm{Cu(In_{1-x}Ga_x)Se_2}\ \text{nanocrystals} + \text{byproducts}$$

The final composition could be easily controlled by the initial ratio of $InCl_3$ and $GaCl_3$, which was relatively hard

Table 5 Comparison of I–V properties of CZTS solar cells with different thickness of absorption layer [52, 53]

R&D group	Thickness (nm)	J_{SC} (mA/cm^2)	V_{oc} (mV)	FF (%)	η (%)
Katagiri et al.	950	7.01	415	50.3	1.46
	1340	3.41	425	26.5	0.384
	1630	1.53	525	26.6	0.214
Wang et al.	650	17.8	587	65	6.81
	660	20.4	620	52	6.63
	900	18.3	640	38	4.40
	1200	14.4	608	28	2.44

Table 6 Synthesis of material by evaporation technique

Methods	Precursor information	Post treatment	Efficiency	Ref.
Sequentiality evaporation	Cu/Sn/Zn stack on Mo/SLG	Annealing in N_2 + H_2S(5 %)	0.66 %	[51]
Sequentiality evaporation	Cu/Sn/ZnS stack on Mo/SLG with diff. total stack thickness	Annealing in N_2 + H_2S(5 %) from 500 to 550 °C	0.214–1.46 %	[52]
Co-evaporation	Cu. Zn, Sn, S co-evaporated on NaF/Mo/SLG	KCN + HCl + KCN etching for 60 s + 120 s + 60 s	5.23 %	[55]
Co-evaporation	Cu, Zn, Sn, S co-evaporated on Mo/SLG with total thickness at 650–1200 nm	Rapid thermal annealing under H_2S + 1 M NaCN etching for 3 min before next step	2.44–6.81 %	[53]
Co-evaporation	**Cu, Zn, Sn, Se co-evaporated on Mo/SLG with 30 nm NaF pre-evaporated for grain-coarsening**	**Selenization at 590 °C under N_2 protection**	**11.6 % (record cell)**	[57]

The row in bold stands for the champion cell among all those reported results

for vacuum case. Later examination demonstrated a CIGS structure. As Ga concentration was increased, lattice constant and optical gap were tuned up [58]. Thus, this method offered a low cost and tunable method of material deposition due to the absence of vacuum and relatively low temperature processing. An efficiency of 3.1 % was achieved under normal atmosphere conditions without high temperature post-annealing [59]. However, the converting efficiency was limited without high temperature post-annealing. Taking $CuIn(S/Se)_2$ for example, the efficiency was reported as 0.24 % [60] without annealing and 3.2 % after annealing in Ar for 1 h [61], even though those two shared similar device structures. This issue still remains as a major problem for nano-crystal based CIGS PVs.

For CZTS/CZTSSe case, one approach is directly starting from chemicals containing the required elements. As a typical example, Carter et al. [62] mixed copper acetylacetonate, zinc acetylacetonate hydrate, tin (IV) bis(acetylacetonate) dichloride in oleylamine before a sulfur/oleylamine mixing. After selenization, a kesterite CZTSSe phase was identified and their best CZTSSe solar cells achieved an efficiency of 8.4 % with a better phase and element ratio control.

Another method is using binary or ternary nano-crystals as precursors since CZTS/CZTSSe has many secondary phases. A common combination using different sulfides was predicted by Herbert et al. in [63] and in the two paths ZnS played a vital role:

Path (1): $Cu_2S/Cu_2S/CuS + ZnS + SnS/SnS_2$ ($\pm$ S) $\rightarrow Cu_2ZnSnS_4$

Path (2): $Cu_2SnS_3 + ZnS \rightarrow Cu_2ZnSnS_4$

The path (2) seems to offer an easier scheme on CZTS/CZTSSe formation (CZTSSe can be formed through another selenization step). However, ZnS also has some disadvantages: It is difficult to distinguish ZnS from CZTS in XRD reference patterns due to the similar lattice parameters. From the comparison in Fig. 10, it is shown that most ZnS peaks are very close to CZTS. Moreover, since ZnS is n-type semiconductor while CZTS is naturally p-type, some residual ZnS exist in the final product may form recombination centers [64]. Thus, some modifications are created. For example, Kavalakkatt et al. [65] tried to replace ZnS by almost intrinsic ZnO nano rod arrays. Their major principle is to deposit Cu_3SnS_4 nano particles on substrates with ZnO nano rod arrays: After electrodeposition of ZnO on fluorine doped SnO_2 coated glass substrate, the sample was dipped into CTS nano particle solution. A 30-minute annealing between 300 and 550 °C is followed to test the influence of temperature. However, various secondary phases such as ZnS, ZnSe and CuSe still cannot be eliminated after annealing. No efficiency data is reported in this work. Cao et al. developed a high efficiency device by introducing normally p-type SnS into the system in path (2): CTS, ZnS and SnS nano particles were prepared and dispersed separately, then mixed and spin-coated. After gaining required thickness the sample was annealed under 560 °C for 20 min under elemental Se and Sn to form the final CZTSSe with the device results shown in Fig. 11 [66].

Hot-injection method is also employed in CZTS/CZTSSe device fabrication and maybe possible to save the workload by eliminating the production of CTS and other nano particle precursors. Typically, the original precursors would directly include copper salt, zinc salt and tin salt, which would be all dissolved in oleylamine. The temperature was 130 °C at the beginning, then raised to 225 °C and injected sulfur-oleylamine solution into the mixture. Then cooled the solution to 80 °C. Guo et al. [68] first reported a low efficiency of 0.73–0.8 % under AM 1.5G illumination. Other starting precursors and device structures were also tested: Steinhagen et al. replaced

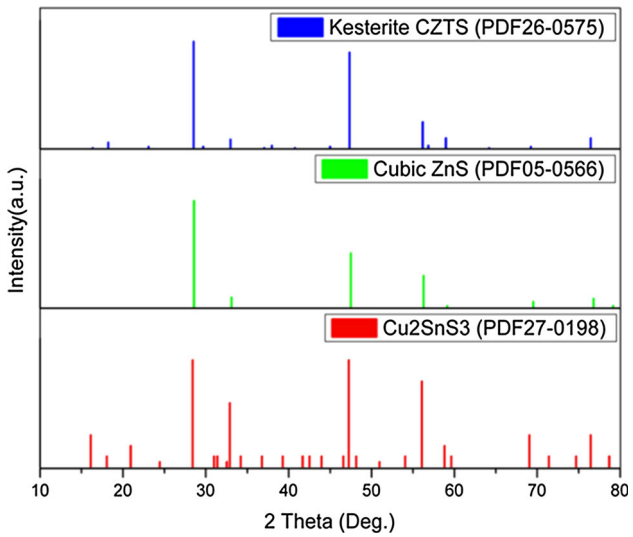

Fig. 10 Comparison of XRD reference patterns of CZTS, ZnS and CTS [67]

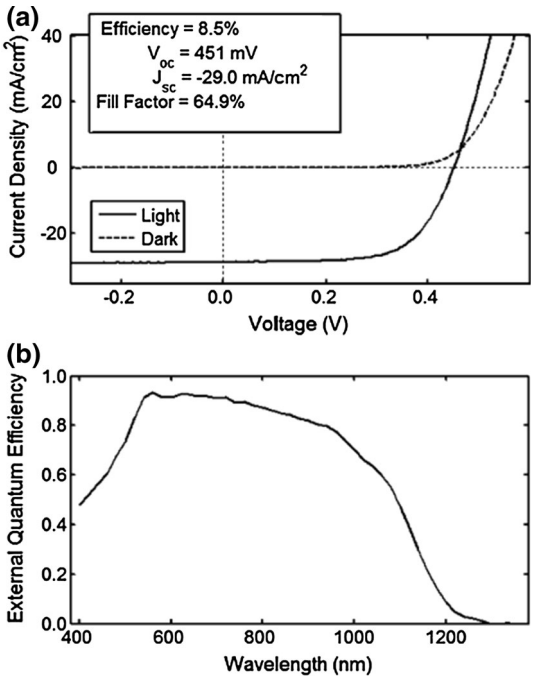

Fig. 11 **a** J–V characteristics and **b** EQE of the same device fabricated by Cao et al. [66]

oleylamine with toluene and after the synthesis and spray-coating on CdS/ZnO-coated ITO glass [69]. After a structure of Au/CZTS/CdS/ZnO/ITO was fabricated, its testing results showed an open-circuit voltage of 321 mV, a short-circuit current density of 1.95 mA/cm^2, a fill factor of 37 %, and an efficiency of 0.23 %. The limited performance of those devices may be due to the inappropriate composition, weak crystal growth or other unknown parameters.

The influence of composition was proved after changing the composition of the cation precursors. In a later report, a mixture with copper poor and zinc rich was applied. A typical composition is 1.332, 0.915, and 0.75 mmol for Cu, Zn and Sn respectively. Oleylamine was still used as solvent. After centrifugation and collection, the final product is proved as $Cu_{1.31\pm0.02}Zn_{0.91\pm0.03}Sn_{0.95\pm0.02}S_4$. Further device followed a standard fabrication structure of SLG/Mo/CZTSSe/CdS/i-ZnO/ITO after a partial selenization under elemental Se in a graphite box between 400 and 500 °C. Finally, a 7.23 % efficiency was achieved after light soaking, which was significantly improved based on the previous result [15]. In addition, this group recently published their upgraded 9.0 % efficient cell based on modification at initial nanoparticle synthesis and selenization parameters, which improved the CZTS uniformity and better grain growth to μm level across the CZTS area as shown in Fig. 12 [70].

Other solvents such as hydrazine was also taken into consideration. The IBM group sets a new mark for CZTSSe solar cells based on hydrazine-based procedure. After dissolving elemental sources in hydrazine, a spin-coating process on Mo/SLG substrate and a following annealing step in the controlled sulfur atmosphere under over 500 °C, a CZTSSe film of 1.5–2.2 μm thickness was formed. The devices still followed a typical structure of SLG/Mo/CZTSSe/CdS/ZnO/ITO/Ni–Al and an additional MgF_2 anti-reflection layer on top of the device [71]. Moreover, a further improvement on hydrazine-pure, particle-free solution enhanced the uniformity of CZTSSe film and the final device performance to the current recorded highest efficiency (12.6 %). Also, the n-type window layer and the TCO layer was better optimized to enlarge the photon-excited carrier collection [18]. Figure 13 displayed the element distributions and indicated the improved device structure.

The solution/'ink'-based method also can be modified to other various coating techniques including spray pyrolysis and doctor-blading. Among them, the earliest trial was on spray pyrolysis. In 1996, Nakayama and Ito [72] first combined copper, zinc and tin chlorides and thiourea together as the precursors. After dissolved all the compounds in water, the mixture was coated on a pre-heated glass substrate. Since the film deposited was examined with a sulfur deficiency, a further sulfurization in Ar + H_2S (5 %) environment was added to tune the element ratio back to the stoichiometric. This process was concluded into a particular chemical formula later as shown below [73]:

$$2CuCl + ZnCl_2 + SnCl_4 + 4SC(NH_2)_2 + 8H_2O \rightarrow Cu_2ZnSnS_4 + 4CO_2 + 8NH_4Cl$$

The optimum substrate temperature was later demonstrated to be at 370 °C with bandgap of 1.43 eV without further

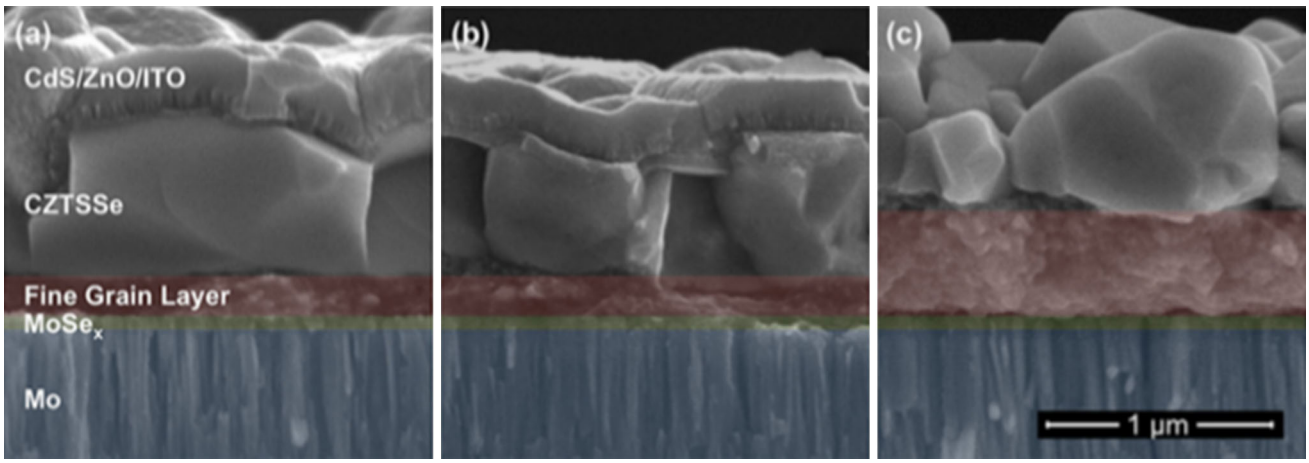

Fig. 12 Cross-section SEM of **a** 9.0 % efficiency device, **b** a sister device selenized at lower temperature and **c** the device selenized with old parameters [70]

annealing or extra sulfurization steps [74]. Figure 14 shows one kind of the typical spray pyrolysis sets. While the left-side generator is optional. Moreover, a selenization process is also applied to help forming CZTSSe films during spray pyrolysis method [76].

Unlike hot-injection method which normally relies on hazardous solvent, the spray pyrolysis has been demonstrated a green path for CZTSSe solar cells. Zeng et al. mixed all three metal chlorides in an acidic aqueous solution. With excess thiourea, the CZTSSe was formed after spray pyrolysis and selenization. Without the negative effect of carbon trace, the uniform CZTSSe layer finally formed a device with 5.1 % efficiency and V_{oc} = 370 mV, J_{sc} = 27.3 mA/cm^2, FF = 50.6 % [77]. A similar research relied on rich Se precursor and a post-sulfurization also achieved an efficiency of 5.8 % [78].

Spin-coating is a relative simple approach without very precise control as spray pyrolysis. It has been widely used in 'ink'-based method, especially the current world champion device from IBM [18]. However, this method needs to repeat for several times to form appropriate film thickness since only a relative thin uniform layer is enabled under the general rotation. Also, it is better to use less toxic solvent than, for example, hydrazine. The original sol–gel could be totally metal chloride [75] or a mixture of soluble metal salts with different anions [76]. In an example, copper chloride, zinc acetate, tin chloride were mixed in 2-methoxyethanol. Thiourea was added with inert gas protection while heating the solution. After spin-coating on Mo/SLG followed by drying and sulfurization in N_2/H_2S mixture, the final film was almost single-phase CZTS with a bandgap of 1.48 eV and the final device showed a J_{sc} of 14.57 mA/cm^2, a Voc of 513 mV, a FF of 40 % and an efficiency of 3.01 % [79]. A similar trial was accomplished

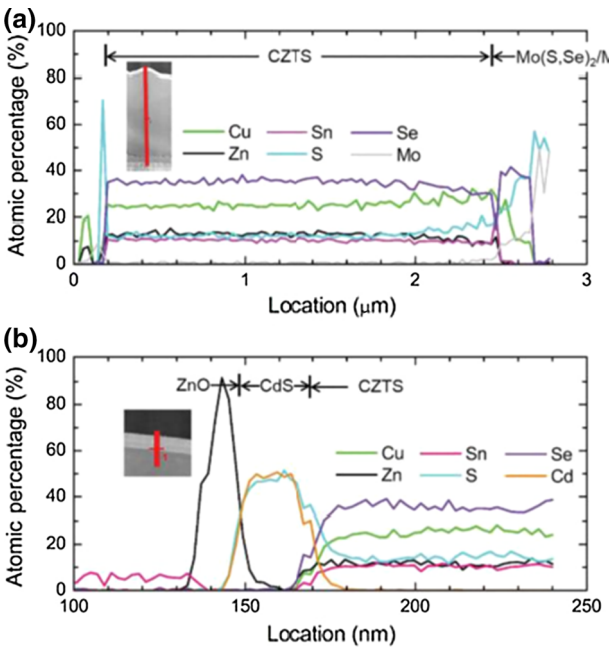

Fig. 13 EDX results on a 12 % CZTSSe device of **a** CZTSSe/Mo area and **b** CZTSSe/CdS/ZnO area [18]

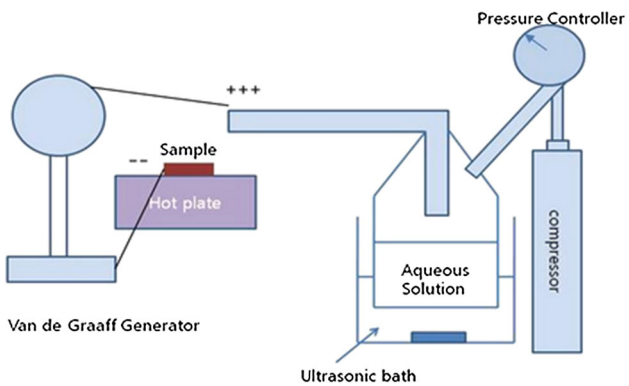

Fig. 14 Schematic of Spray pyrolysis process [75]

with lower sulfurization temperature at 300 °C, where CZTS films has lowest resistivity and highest carrier concentration and mobility. However, the efficiency only reached 1.45 % with a FF less than 30 % possibly due to high series resistance, extra sulfur loss and inadequate CZTS grain growth [80].

As the holder of current CZTS/Se champion cell, those non-vacuum methods showed clear advantages over the vacuum approaches. The solution synthesis and hot injection methods showed more efficient way on CZTS/Se synthesis. The successful investigation on CZTS/Se spray pyrolysis and spin-coating offered alternative choices for potential large-scale manufacturing in the future. Compared with other solution-based methods, more environmental-friendly solvent, especially water, had been proved suitable for CZTS/Se cell fabrication. Detailed information could be found at Table 7. Even though high temperature sulfurization/selenization was still required in order to produce high-efficient cells, future works may focus on sol–gels with "green" solvents or conditions, rather than those most common-used hydrazine or oleylamine, that might help forming CZTS/Se during the deposition, i.e. one-step CZTS/Se formation.

Doctor-blading could be considered as the upgrade version of general sol–gel methods. To form thin films especially on larger surface, the blade moves relative to the substrate. Figure 15 showed the basic working principle of this method. The film thickness could be roughly controlled by arranging multiple blades. However, it is not only the distance between blade and substrate but also the surface tension, dynamic viscosity and solvent evaporation could affect the final thickness [81]. In an example, the mixed CZT source in oleylamine was heated while adding thiourea solution (in OLA also) in order to form CZTS colloids. The whole mixture was deposited on Mo/glass by repeating doctor-blading methods. After sulfurization, the device was assembled with CdS, i-ZnO, AZO and Ag top grid. The device showed an immediate efficiency of 2.00 %. With extending light soaking, the efficiency slowly increased to 2.29 % [82]. From Fig. 16 [81], it could be inferred that better morphological control and higher recombination rate are still the barrier for further application of doctor-blading.

Doctor-blading gives change to form thicker absorption layer within less deposition times especially with spin-coating. Also, doctor-blading has more freedom on choosing deposition areas. However, their similar point was that both methods still have room to improve on the choice of solvents and sol–gel viscosity. Also, surface roughness could be another problem if the blade height cannot be controlled precisely, which is as shown in Fig. 16 [81].

5.3.1 *Electro-deposition*

Compared with solution-based method, electro-deposition is more mature and already has many industrial applications, e.g. the copper deposition onto the IC board. Similarly, in the CZTS/CZTSSe case, the initial trial was still focused on forming different pure metal layers, then sent the sample into the furnace to finish sulfurization under sulfur atmosphere. The report from Scragg et al. [83] developed this procedure and demonstrated a low efficiency of 0.8 %. Another Zn/Cu/Sn/Cu stack, even required additional KCN etching to remove all excess copper sulfide phase, improved the efficiency to 3.2 % [84].

Later, Schurr et al. worked on almost same metal stack and similar procedure except some different parameters. However, the stack was fabricated by co-electrodeposition, one step only. Their in situ XRD result indicated two different set of mechanisms on CZTS synthesis while final results remain the same: CZTS is synthesized through CTS and ZnS [85]. A conversion efficiency of 3.4 % (Voc = 563 mV, Jsc = 14.8 mA/cm^2, FF = 41 %; device area = 0.5 cm^2) was obtained by using similar process [86]. The detail information of reaction mechanism is shown below [67, 85]:

For copper-poor case,

$$Cu_6Sn_5 + S \rightarrow SnS_2 + Cu_{2-x}S + Cu_3Sn;$$

$$2Cu_2S + SnS_2 + 2S \rightarrow Cu_4SnS_6;$$

$$Cu_4SnS_6 \rightarrow 2Cu_{2-x}S + SnS_2(\text{melted}) + 2S;$$

$$Cu_{2-x}S + SnS_2(\text{melted}) \rightarrow Cu_2SnS_3;$$

$$Cu_2SnS_3 + ZnS \rightarrow Cu_2ZnSnS_4;$$

For copper-rich case,

$$2Cu_3Sn + 7S \rightarrow 3Cu_{2-x}S + 2SnS_2;$$

$$2CuZn + 3S \rightarrow Cu_{2-x}S + 2ZnS;$$

$$Cu_{2-x}S + SnS_2 \rightarrow Cu_2SnS_3;$$

$$Cu_2SnS_3 + ZnS \rightarrow Cu_2ZnSnS_4;$$

Current record efficiency of CZTS thin films deposited via selenization on precursors stack is 8.2 % as noticed [87]. The formation of metal stacks has little highlight. A complex multiple etching process ($KMnO_4/H_2SO_4$ + - Na_2S + $(NH_4)_2S$) was applied to completely remove the secondary phases formed in selenization with presence of Sn powder to reduce Sn loss.

Meanwhile, deposition without as-prepared metal stack also attract some attention since this process may become another one-step method. Pawar et al. [88] first demonstrated the possibility by applying a typical three-electrode electrochemical cell structure into an aqueous solution

Table 7 A full list of solution-based synthesis

Detailed method	Precursor information	Post treatment	Efficiency	Ref.
Solution synthesis/spray deposition	0.1 M CuCl and 0.1 M $InCl_3$ in OLA, heated under 110 °C for 10 min in N_2 + 1 M Se in TPB, then heat for 10 min under 240 Co in N_2. Re-dispersed in ethanol	None	3.1 %	[59]
Solution synthesis/drop casting	CuCl:$InCl_3$:Se = 1:1:2 (mol) in OLA. System was heated under 240 °C for 4 h in vacuum and quenched with chloroform and separated by ethanol	None	0.24 %	[60]
Solution synthesis/drop casting	CuCl, $InCl_3$, Se with OLA heated in 265/285 °C in Ar. Nano-crystals formed with hexane and ethanol & re-dispersed in toluene	Sintering in Ar and Se under 500 °C for 1 h	3.2 %	[61]
Solution synthesis/doctor blading	Mixed $Cu(acac)_2$, $Zn(acac)_2{\cdot}xH_2O$, $Sn(acac)_2Cl_2$ in OLA + Sulfur/OLA, heat under 225/250 °C with Ar protection	Sintered in Se under 500 °C, 20 min	6.7–8.4 %	[62]
Solution synthesis/spin coating	Pre-synthesized CTS, SnS, ZnS nano-particles in hexanethiol were mixed	Selenization at 560 °C for 20 min	8.5 %	[66]
Hot injection/drop casting	$Cu(acac)_2$, $Zn(acac)_2$, $Sn(acac)_2Br_2$ in OLA, 1 M S/OLA is injected at 225 °C and total mixture was heated for 30 min. Final particles was in toluene	Selenization in graphite box under 400–500 °C	0.73–0.8 %	[68]
Hot injection/spray coating	$Cu(acac)_2$, $Zn(ac)_2$, $SnCl_2$ and S were added into OLA with N_2 protection. System was heated at 280 °C for 1 h	None	0.23 %	[69]
Hot injection/doctor blading	$Cu(acac)_2$, $Zn(acac)_2$, $Sn(acac)_2Br_2$ in OLA, 1 M S/OLA is injected at 225 °Cand heated for 30 min. Cu:Zn:Sn = 1.332:0.915:0.75	Selenization in 500 °C for 20 min	7.2 %	[15]
Hot injection/doctor blading	Add $Cu(acac)_2$, $Zn(acac)_2{\cdot}xH_2O$, $Sn(acac)_2Cl_2$ in OLA under Ar + 1 M S/OLA injection at 250 °C and react for 20 s	Selenization in 500 °C for 20 min	9.0 (9.8) % For total (active) area	[70]
Solution synthesis/spin coating	**Cu/(Zn + Sn) = 0.8 and Zn/Sn = 1.1 with all precursors in hydrazine**	**Annealing in Sulfur under more than 500 °C**	**12.6 % (record cell)**	[18]
Spray pyrolysis	Dissolve $CuCl_2{\cdot}2H_2O$, $ZnCl_2$, $SnCl_2{\cdot}2H_2O$ in water and HCl, Cu:Zn:Sn = 100:78:62	Selenization in 520 °C for 12 min	5.1 %	[77]
Spray pyrolysis	Dissolve $Cu(NO_3)_2$, $Zn(NO_3)_2$, $Sn(CH_3SO_3)_2$, $SC(NH_2)_2$ in water and HCl with pH ~ 1.5	Annealing with Sulfur under 580-600 °C for 10-50 min	5.8 %	[78]
Sol–gel spin coating	Add copper chloride, zinc acetate, tin chloride in 2-methoxyethanol, add thiourea into solution at 45 °C. Cu:Zn:Sn:S = 8:5:4:32	Annealing with H_2S in 525/550/575 °C	3.01 % (annealed in 575 °C)	[79]
Sol–gel spin coating	Add $Cu(ac)_2{\cdot}H_2O$, $Zn(ac)_2$, $SnCl_2$, Thiourea in 2-methoxyethanol under 45 °C. Cu:Zn:Sn:S = 9:6:5:40	Annealing with Sulfur in 580 °C for 1 h	1.45 %	[80]
Hot Injection/Doctor Blading	$Cu(acac)_2$, $Zn(acac)_2{\cdot}xH_2O$, $SnCl_2$ were into OLA + 1 M S/OLA added at 240 °C and react 30 min under Ar	Annealing with H_2S in 530/550/570 °C for 30 min	2.29 %	[82]

The row in bold stands for the champion cell among all those reported results

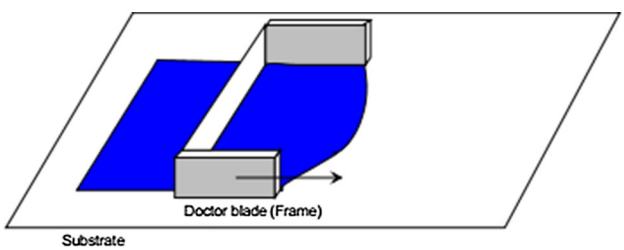

Fig. 15 Schematic drawing of doctor-blade coating [80]

including $CuSO_4$, $ZnSO_4$, $SnSO_4$ and $Na_2S_2O_3$. After the deposition, the sample were annealed in argon at 550 °C to strengthen the film and remove water. The final product had a bandgap of 1.5 eV. Ge et al. [89] added extra complex agents $Na_3C_6H_5O_7$ and $C_4H_4K_2O_6$ and after selenization, they successfully synthesized CZTSSe with the designed S/Se ratio. However, until now no reported device efficiency could be found.

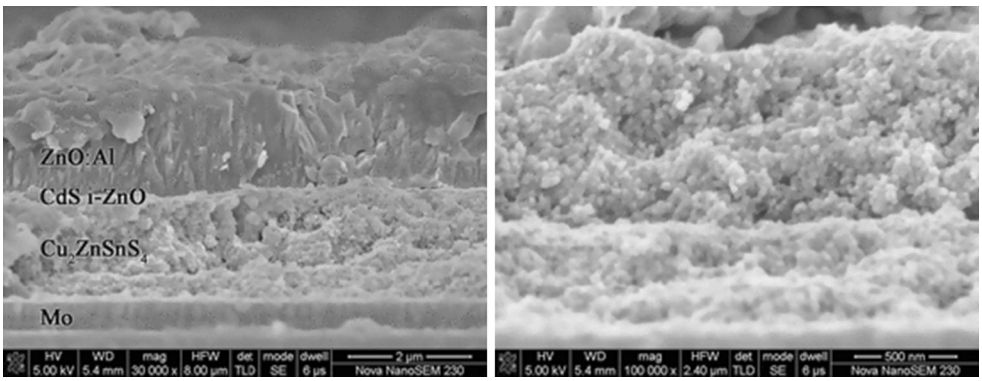

Fig. 16 Cross-sectional SEM and a closed magnification of the doctor-bladed CZTS device [81]

Table 8 A list of electro-deposition based synthesis

Methods	Details of initial set-up	Post treatment	Efficiency	Ref.
3-electrode cell deposition	Cu/Sn/Zn stack. NaOH appeared in Cu/Sn deposition. Zn formed with Hydrion buffer	Sulfurized with Ar in 550 °C with 40 °C/min temp ascending	0.8 %	[83]
3-electrode cell deposition	Cu/Sn/Zn stack Cu:NaOH + $CuSO_4$ + Sorbitol + Empigen BB Sn:$Sn(SO_3CH_3)_2$ + HCH_3SO_3+ Empigen BB Zn:$ZnSO_4 \cdot 7H_2O$ + Hydrion buffer	Sulfurized with H_2(10 %)/N_2 in 575 °C for 2 h	3.2 %	[84]
Electro-chemical Co-deposition	Cu + Zn + Sn mixture stack Evaporated S layer on stack	Annealed in 630 °C for 5 min, with 0.8 K/min temp ascending	3.4 %	[86]
Sequential Electro-deposition	**Cu/Sn/Zn stack.** **Cu/Zn + Sn = 0.74, Zn/Sn = 1.25** **Followed with air-filled annealing at 200 °C for 30–120 min**	**Selenized with Sn powder in vacuum under 350 °C, 30 min + 550 °C, 15 min** **Step-by-step Etching in $KMnO_4$/ H_2SO_4 + Na_2S + $(NH_4)_2S$ before CdS coating**	**8.2 % (record cell)**	[87]

The row in bold stands for the champion cell among all those reported results

Similar as the sputtering, electro-deposition also requires a formation of metal precursors before continuing with high-temperature sulfurization, as shown in Table 8. Thus, the thickness for each layer in the stack becomes important for the final cation ratio as well as the CZTS/Se formation. However, a more complicated electrolyte bath is required especially for co-deposition. In addition, since the CZTSe was demonstrated a good enhancement on cell efficiency (see the record results for sputtering), a similar selenization step may assessed as the post treatment for electro-deposited CZT stacks.

5.3.2 Powder metallurgy approach

Powder metallurgy approaches have been applied for producing small particles for a long time. Some typical methods are ball-milling and sintering (solid-state, liquid-phase, reactive, pressure-assisted and etc.) [90]. Generally, the synthesis approach would include multiple process rather than only one: ball-milling would first roughly decreased the particle size, than using sintering to initiate the reaction or re-crystallization, then the particle would re-grow to a more condensed and uniform situation. For liquid-phase sintering, choosing proper sintering aids has a significant influence on the liquid viscosity and transportation ability for the aimed particles. Thus, the film quality would be largely affected. In an example, Sb_2S_3 and Te were chosen as the sintering aids, while CuS, ZnS, SnS and another set of Cu_2Se, ZnSe, $SnSe_2$ in the initial reactive sintering at 600 °C for 1 h [91]. The final product were CZTSSe pellets according to the XRD and Raman shift. The bandgap, carrier concentration, mobility and etc. can be tuned through S/Se ratio. However, this group didn't report a device conversion efficiency. Krustok et al. [92] also applied metal binaries as the starting materials (CuSe, ZnSe(S), SnSe and elemental Se). After the isothermal recrystallization process, mono-grain CZTSSe was synthesized. The solar cell based on as-synthesized 56–63 μm

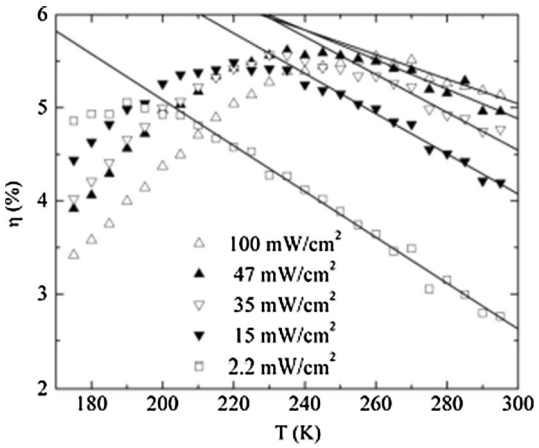

Fig. 17 Temperature dependence of the relative efficiency of a CZTSSe mono-grain solar cell illuminated with different light intensities from low temperature to room temperature [92]

CZTSSe powders showed a strong influence of temperature on the device efficiency shown in Fig. 17. From this figure, it is observed that there is a peak efficiency at a point lower than the room temperature. The peak point shifted to cold region while incident power reducing. With temperature decreasing, the efficiency dropped down simultaneously due to lower driving force. However, when temperature increasing, the efficiencies were also kept decreasing because of the temperature effect on the fill factors [92].

In powder metallurgy method, direct elemental precursors could be also used in the synthesis of CZTSSe. A Cu–Zn–Sn metal alloy was applied as the starting materials with an element ratio of Cu:Zn:Sn = 1.67:1.03:1. Elemental S and Se also participated the reaction in evacuated quartz ampoules and mixed with liquid KI as sintering aids. Cu_2S, SnSe and ZnSe powders were applied to modify the S/Se ratio [93]. After the reaction, the samples were annealed under different temperatures and later examination claimed a product of mono-grain CZTSSe. This approach was also applicable on the synthesis of CZTS and CZTSe. Moreover, with a device structure of graphite/CZTSe/CdS/ZnO/AZO, the efficiency was reported as 2.16 [94] and 5.9 % when using CZTSSe (S/Se = 3) to replace CZTSe [95]. Since little literature about using such method can be found to the best of our knowledge, it is hard to summarize the advantages and disadvantages. However, if a solid-state CZTSSe could be steady reproduced, a better bulk CZTSSe target might be expected to assist CZTSSe film sputtering.

6 Conclusion

Kesterite-related CZTS/CZTSe/CZTSSe is considered as an alternative material system to CIGS series which have limited applications due to the abundant elements, competitive lattice constant and electrical/optical properties. Thus, it is possible to fabricate a CZTS solar cell device by simply replacing CIGS by CZTS with other structures remain the same. CZTS series also have a suitable bandgap for solar cell application and by tuning the S/Se ratio, the bandgap engineering could be controlled from about 1.0–1.5 eV. Many approaches and precursor compositions including elemental, binary and ternary precursors have been developed on the fabrication of CZTS/CZTSSe solar cell devices. Sputtering, evaporation, solution-based approach, electro-deposition and metallurgy are all demonstrated available on CZTS/Se solar cell fabrication. The champion data for each methods are: 8.1 % for sputtering, 11.6 % for evaporation, 12.6 % for solution-based approaches (also the current highest record), 8.2 % for electro-deposition and 5.9 % for metallurgy method. Among them, the Cu-poor and Zn-rich under solution-based approach seems to be the mainstream. However, the top CZTSSe lab device (12.6 %) still lays a great gap with performance from either top CIGSSe lab cells (22.3 %) or the record module efficiency (16.5 %). Thus, many improvements are waiting for CZTS/Se system before it could really comparable with CIGS/Se or CdTe cells. Otherwise, the best position for CZTS/Se is being a permanent substitution for absorption layer of thin film solar cells.

At present, numerous problems on CZTS/Se thin film solar cells are still remained. Among them, precisely controllability of composition in CZTS/Se is very challenging. The optimum region for CZTS phase is much smaller than CIGS and lots of secondary phases may appear during the CZTS formation. These phases are not only block the formation and identification of CZTS/Se phase (such as the similarity of XRD between ZnS and CZTS), but also increased extra steps in CZTS/Se cell fabrication (e.g. highly-toxic 10 % KCN etching becomes common in order to remove the extra Cu_xS phase). Second, to assist a better phase control, reaction mechanisms or dynamics of CZTS/CZTSe becomes more necessary in order to sort out the best precursor set. The effect of diffused sodium (mainly from SLG substrate diffusion and sodium compound solution treatment on CZTS/Se layer) are also deserved for further discussion. Besides, the selenization/sulfurization still serves as a major contribution to the re-crystallization of CZTS/CZTSe and such step mostly works in a temperature region higher than 500 °C. If not sintered or sintered under a lower temperature, a CZTS/CZTSe device mostly returned an efficiency lower than 1 % (at most around 3 %) rather than the current record of 12.6 %. By solving these problems, the ideal fabrication method with least trimming steps will keep approaching to us. Also, the CZTS/Se solar cell could be fabricated on flexible polymer-based substrate if post treatment temperature could be

decreased. Thus, wider application of CZTS/Se solar cell may become possible. Due to the similarity of CZTS and CIGS system, some solutions and experience for improving CIGS device performance may also applicable for CZTS/CZTSSe case.

References

1. SEIA/GTM Research: U.S. Solar Market®, Q3 2015, Executive Summary
2. Global Market Outlook for Solar Power, 2015-2019, Solar Power Europe
3. Staff writer, Pricing Sunshine, The Economist, Retrieved 2012-12-28
4. Photovoltaics Report, Fraunhofer Institute for Solar Energy Systems, ISE, 2015
5. S. Abermann, Sol. Energy **94**, 37–70 (2013)
6. M. Taguchi, A. Yano, S. Tohoda, K. Matsuyama, Y. Nakamura, T. Nishiwaki, K. Fujita, E. Maruyama, IEEE J Photovolt **4**, 96–99 (2014)
7. P. Jackson, D. Hariskos, R. Wuerz, O. Kiowski, A. Bauer, T.M. Friedlmeier, M. Powalla, Phys. Status Solidi RRL **9**, 28–31 (2015)
8. http://investor.firstsolar.com/releasedetail.cfm?ReleaseID=895118
9. Z. Li, Y. Liu, W. Liu, Z. Li, L. Cheng, X. Qin, X. Li, Z. Zhou, Y. Zhang, Q. He, Y. Sun, Mater. Res. Express **2**, 046403 (2015)
10. S.R. Taylor, S.M. McLennan (Blackwell Scientific Publication, Oxford 1985) 1-312
11. G. Phipps, C. Mikolajczak, T. Guckes, Renew. Energy Focus **9**, 56–59 (2008)
12. K. Ito, T. Nakazawa, Jpn. J. Appl. Phys. **27**, 2094 (1988)
13. T.M. Friedlmeier, N. Wieser, T. Walter, H. Dittrich, H.W. Schock, *Proceedings of the 14th European Photovoltaic Solar Energy Conference*, 1997
14. H. Katagiri, K. Jimbo, W.S. Maw, K. Oishi, M. Yamazaki, H. Araki, A. Takeuchi, Thin Solid Films **517**, 2455–2460 (2009)
15. Q. Guo, G.M. Ford, W.C. Yang, B.C. Walker, E.A. Stach, H.W. Hillhouse, R. Agrawal, J. Am. Chem. Soc. **132**, 17384–17386 (2010)
16. I. Repins, C. Beall, N. Vora, C. DeHart, D. Kuciauskas, P. Dippo, B. To, J. Mann, W.C. Hsu, A. Goodrich, R. Noufi, Sol. Energy Mater. Sol. Cells **101**, 154–159 (2012)
17. D. Aaron, R. Barkhouse, O. Gunawan, T. Gokmen, T.K. Todorov, D.B. Mitzi, Prog. Photovoltaics Res. Appl. **20**, 6–11 (2012)
18. W. Wang, M.T. Winkler, O. Gunawan, T. Gokmen, T.K. Todorov, Y. Zhu, D.B. Mitzi, Adv. Energy Mater. **4**, 1301465 (2014)
19. S.Y. Chen, X.G. Gong, A. Walsh, S.H. Wei, Appl. Phys. Lett. **94**, 041903 (2009)
20. J.E. Bernard, L.G. Ferreira, S.H. Wei, A. Zunger, Physical Review B **38**, 6338 (1988)
21. R. Magri, S.H. Wei, A. Zunger, Phys. Rev. B **42**, 11388 (1990)
22. C. Persson, J. Appl. Phys. **107**, 053710 (2010)
23. S. Siebentritt, S. Schorr, Prog. Photovoltaics Res. Appl. **20**, 512–519 (2012)
24. D.B. Mitzi, O. Gunawan, T.K. Todorov, K. Wang, S. Guha, Sol. Energy Mater. Sol. Cells **95**, 1421–1436 (2011)
25. S. Delbos, EPJ Photovoltaics **3**, 35004 (2012)
26. R.A. Wibowo, H. Yoo, A. Hölzing, R. Lechner, S. Jost, J. Palm, M. Gowtham, B. Louis, R. Hock, Thin Solid Films **535**, 57–61 (2013)
27. F.J. Fan, L. Wu, M. Gong, G. Liu, Y.X. Wang, S.H. Yu, S.Y. Chen, L.W. Wang, X.G. Gong, ACS Nano **7**, 1454–1463 (2013)
28. X. Song, X. Ji, M. Li, W. Lin, X. Luo, H. Zhang, Int. J. Photoenergy **2014**, 613173 (2014)
29. S.Y. Chen, X.G. Gong, A. Walsh, S.H. Wei, Phys. Rev. B **79**, 165211 (2009)
30. J. He, L. Sun, S.Y. Chen, Y. Chen, P.X. Yang, J.H. Chu, J. Alloy. Compd. **511**, 129–132 (2012)
31. T.K. Todorov, K.B. Reuter, D.B. Mitzi, Adv. Mater. **22**, 156–159 (2010)
32. J. He, L. Sun, N.F. Ding, H. Kong, S.H. Zuo, S.Y. Chen, Y. Chen, P.X. Yang, J.H. Chu, J. Alloy. Compd. **529**, 34–37 (2012)
33. B. Welber, M. Cardona, C.K. Kim, S. Rodriguez, Phys. Rev. B **12**, 5729 (1975)
34. E. Ghahramani, J.E. Sipe, Phys. Rev. B **40**, 12516 (1989)
35. S.Y. Chen, J. Yang, X. Gong, A. Walsh, S. Wei, Phys. Rev. B **81**, 245204 (2010)
36. J.W. Lee, J.D. Cohen, W.N. Shafarman, Thin Solid Films **480–481**, 336–340 (2005)
37. P.A. Fernandes, P.M.P. Salomé, A.F. da Cunha, B. Schubert, Thin Solid Films **519**, 7382–7385 (2011)
38. F. Liu, K. Zhang, Y. Lai, J. Li, Z. Zhang, Y. Liu, Electrochem. Solid-State Lett. **13**, 379–381 (2010)
39. R. Haight, A. Barkhouse, O. Gunawan, B. Shin, M. Copel, M. Hopstaken, D.B. Mitzi, Appl. Phys. Lett. **98**, 253502 (2011)
40. J.M. Raulot, C. Domain, J.F. Guillemoles, J. Phys. Chem. Solids **66**, 2019–2023 (2005)
41. A. Opanasyuk, D. Kurbatov, M. Ivashchenko, I.Y. Protsenko, H. Cheong, J. Nano Electronic Phys. **4**, 01024 (2012)
42. A. Weber, R. Mainz, H.W. Schock, J. Appl. Phys. **107**, 013516 (2010)
43. R. Lechner, S. Jost, J. Palm, M. Gowtham, F. Sorin, B. Louis, H. Yoo, R.A. Wibowo, R. Hock, Thin Solid Films **535**, 5–9 (2013)
44. A. Fairbrother, X. Fontané, V. Izquierdo-Roca, M. Espíndola-Rodríguez, S. López-Marino, M. Placidi, L. Calvo-Barrio, A. Pérez-Rodríguez, E. Saucedo, Sol. Energy Mater. Sol. Cells **112**, 97–105 (2013)
45. J. Márquez, M. Neuschitzer, M. Dimitrievska, R. Gunder, S. Haass, M. Werner, Y.E. Romanyuk, S. Schorr, N.M. Pearsall, I. Forbes, Sol. Energy Mater. Sol. Cells **144**, 579–585 (2016)
46. K. Jimbo, R. Kimura, T. Kamimura, S. Yamada, W.S. Maw, H. Araki, K. Oishi, H. Katagiri, Thin Solid Films **515**, 5997–5999 (2007)
47. H. Katagiri, K. Jimbo, M. Tahara, H. Araki, K. Oishi, Mater. Res. Soc. Symp. Proc. **1165**, M04-01 (2009)
48. L. Grenet, S. Bernardi, D. Kohen, C. Lepoittevin, S. Noel, N. Karst, A. Brioude, S. Perraud, H. Mariette, Sol. Energy Mater. Sol. Cells **101**, 11–14 (2012)
49. J. He, L. Sun, K. Zhang, W. Wang, J. Jiang, Y. Chen, P. Yang, J. Chu, Appl. Surf. Sci. **264**, 133–138 (2013)
50. Y.P. Lin, Y.F. Chi, T.E. Hsieh, Y.C. Chen, K.P. Huang, J. Alloy. Compd. **654**, 498–508 (2016)
51. H. Katagiri, N. Sasaguchi, S. Hando, S. Hoshino, J. Ohashi, T. Yokota, Sol. Energy Mater. Sol. Cells **49**, 407–414 (1997)
52. H. Katagiri, K. Saitoh, T. Washio, H. Shinohara, T. Kurumadani, S. Miyajima, Sol. Energy Mater. Sol. Cells **65**, 141–148 (2001)
53. K. Wang, O. Gunawan, T. Todorov, B. Shin, S.J. Chey, N.A. Bojarczuk, D. Mitzi, S. Guha, Appl. Phys. Lett. **97**, 143508 (2010)
54. W.C. Hsu, I. Repins, C. Beall, C. DeHart, G. Teeter, B. To, Y. Yang, R. Noufi, Sol. Energy Mater. Sol. Cells **113**, 160–164 (2013)
55. T. Prabhakar, N. Jampana, Sol. Energy Mater. Sol. Cells **95**, 1001–1004 (2011)
56. T. Mise, S. Tajima, T. Fukano, K. Higuchi, T. Washio, K. Jimbo, H. Katagiri, Prog. Photovoltaics Res. Appl. **24**, 1009–1015 (2016)

57. Y.S. Lee, T. Gershon, O. Gunawan, T.K. Todorov, T. Gokmen, Y. Virgus, S. Guha, Adv. Energy Mater. **5**, 1401372 (2015)
58. V.A. Akhavan, B.W. Goodfellow, M.G. Panthani, C. Steinhagen, T.B. Harvey, C.J. Stolle, B.A. Korgel, J. Solid State Chem. **189**, 2–12 (2012)
59. V.A. Akhavan, M.G. Panthani, B.W. Goodfellow, D.K. Reid, B.A. Korgel, Energy Express **18**, A411–A420 (2010)
60. M.G. Panthani, V. Akhavan, B. Goodfellow, J.P. Schmidtke, L. Dunn, A. Dodabalapur, P.F. Barbara, B.A. Korgel, J. Am. Chem. Soc. **130**, 16770–16777 (2008)
61. Q. Guo, S.J. Kim, M. Kar, W.N. Shafarman, R.W. Birkmire, E.A. Stach, R. Agrawal, H.W. Hillhouse, Nano Lett. **8**, 2982–2987 (2008)
62. N.J. Carter, W.C. Yang, C.K. Miskin, C.J. Hages, E.A. Stach, R. Agrawal, Sol. Energy Mater. Sol. Cells **123**, 189–196 (2014)
63. F. Hergert, R. Hock, Thin Solid Films **515**, 5953–5956 (2007)
64. P.M.P. Salome, J. Malaquias, P.A. Fernandes, M.S. Ferreira, J.P. Leitao, A.F. da Cunha, J.C. Gonzalez, F.N. Matinaga, G.M. Ribeiro, E.R. Viana, Sol. Energy Mater. Sol. Cells **95**, 3482–3489 (2011)
65. J. Kavalakkatt, X. Lin, K. Kornhuber, P. Kusch, A. Ennaoui, S. Reich, MCh. Lux-Steiner, Thin Solid Films **535**, 380–383 (2013)
66. Y. Cao, M.S. Denny Jr., J.V. Caspar, W.E. Farneth, Q. Guo, A.S. Ionkin, L.K. Johnson, M. Lu, I. Malajovich, D. Radu, H.D. Rosenfeld, K.R. Choudhury, W. Wu, J. Am. Chem. Soc. **134**, 15644–15647 (2012)
67. M. Jiang and X. Yan, Solar Cells-Research and Application Perspectives, Chapter 5 (2013)
68. Q. Guo, H.W. Hillhouse, R. Agrawal, J. Am. Chem. Soc. **131**, 11672–11673 (2009)
69. C. Steinhagen, M.G. Panthani, V. Akhavan, B. Goodfellow, B. Koo, B.A. Korge, J. Am. Chem. Soc. **131**, 12554–12555 (2009)
70. C.K. Miskin, W.C. Yang, C.J. Hages, N.J. Carter, C.S. Joglekar, E.A. Stach, R. Agrawal, Prog. Photovoltaics Res. Appl. **23**, 654–659 (2015)
71. T.K. Todorov, J. Tang, S. Bag, O. Gunawan, T. Gokmen, Y. Zhu, D.B. Mitzi, Adv. Energy Mater. **3**, 34–38 (2013)
72. N. Nakayama, K. Ito, Appl. Surf. Sci. **92**, 171–175 (1996)
73. N. Kamoun, H. Bouzouita, B. Rezig, Thin Solid Films **515**, 5949–5952 (2007)
74. Y.B.K. Kumar, P.U. Bhaskar, G.S. Babu, V.S. Raja, Phys. Status Solidi A **207**, 149–156 (2010)
75. SNE Research, CZTS (universal element-used in free low-cost CIS based) thin-film solar cell development trends-Part. 2 http://www.sneresearch.com/eng/info/show.php?c_id=4970&pg=5&s_sort=&sub_cat=&s_type=&s_word=
76. H. Yoo, J. Kim, Sol. Energy Mater. Sol. Cells **95**, 239–244 (2011)
77. X. Zeng, K.F. Tai, T. Zhang, C.W.J. Ho, X. Chen, A. Huan, T.C. Sum, L.H. Wong, Sol. Energy Mater. Sol. Cells **124**, 55–60 (2014)
78. T.H. Nguyen, W. Septina, S. Fujikawa, F. Jiang, T. Harada, S. Ikeda, RSC Adv. **5**, 77565–77571 (2015)
79. G.L. Agawane, A.S. Kamble, S.A. Vanalakar, S.W. Shin, M.G. Gang, J.H. Yun, J. Gwak, A.V. Moholkar, J.H. Kim, Mater. Lett. **158**, 58–61 (2015)
80. R. Liu, M. Tan, X. Zhang, J. Chen, S. Song, W. Zhang, J. Alloy. Compd. **655**, 124–129 (2016)
81. A. Berni, M. Mennig and H. Schmidt, Sol-gel technologies for glass producers and users, 2.2.8 doctor blade
82. E. Gu, C. Yan, F. Liu, Y. Liu, Z. Su, K. Zhang, Z. Chen, J. Li, Y. Liu, J. Mater. Sci.: Mater. Electron. **26**, 1932–1939 (2015)
83. J.J. Scragg, P.J. Dale, L.M. Peter, G. Zoppi, I. Forbes, Phys. Status Solidi B **245**, 1772–1778 (2008)
84. J.J. Scragg, D.M. Berg, P.J. Dale, J. Electroanal. Chem. **646**, 52–59 (2010)
85. R. Schurr, A.H. Olzing, S. Jost, R. Hock, T. Voß, J. Schulze, A. Kirbs, A. Ennaoui, M. Lux-Steiner, A. Weber, I.K. Otschau, H.W. Schock, Thin Solid Films **517**, 2465–2468 (2009)
86. A. Ennaoui, M. Lux-Steiner, A. Weber, D. Abou-Ras, I.K. Otschau, H.W. Schock, R. Schurr, A.H. Olzing, S. Jost, R. Hock, T. Voß, J. Schulze, A. Kirbs, Thin Solid Films **517**, 2511–2514 (2009)
87. L. Vauche, L. Risch, Y. Sánchez, M. Dimitrievska, M. Pasquinelli, T.G. de Monsabert, P.P. Grand, S.J. Ferrer, E. Saucedo, Prog. Photovoltaics Res. Appl. **24**, 38–51 (2016)
88. S.M. Pawar, B.S. Pawar, A.V. Moholkar, D.S. Choi, J.H. Yun, J.H. Moon, S.S. Kolekar, J.H. Kim, Electrochim. Acta **55**, 4057–4061 (2010)
89. J. Ge, S.H. Zuo, J.C. Jiang, J.H. Ma, L.H. Yang, P.X. Yang, J.H. Chu, Appl. Surf. Sci. **258**, 7844–7848 (2012)
90. R.M. German, *Sintering Theory and Practice* (John Wiley & Sons Inc, New York, NY, 1996)
91. M. Tsega, D.H. Kuo, J. Alloy. Compd. **557**, 142–146 (2013)
92. J. Krustok, R. Josepson, M. Danilson, D. Meissner, Sol. Energy **84**, 379–383 (2010)
93. K. Muska, M. Kauk-Kuusik, M. Altosaar, M. Pilvet, M. Grossberg, O. Volobujeva, Energy Procedia **10**, 203–207 (2011)
94. E. Mellikov, D. Meissner, T. Varema, M. Altosaar, M. Kauk, O. Volobujeva, J. Raudoja, K. Timmo, M. Danilson, Sol. Energy Mater. Sol. Cells **93**, 65–68 (2009)
95. K. Timmo, M. Altosaar, J. Raudoja, K. Muska, M. Pilvet, M. Kauk, T. Varema, M. Danilson, O. Volobujeva, E. Mellikov, Sol. Energy Mater. Sol. Cells **94**, 1889–1892 (2010)